applied optics

Laser communication pointing errors caused by bending deformation of the altitude axis of a T-shaped altitude-azimuth mount

Shaohang Ding,[1,2,*] **Xiaogang San,**[1] **Shijie Gao,**[1] **Yingxue Ni,**[1] **and Jing Wang**[1]

[1]*Changchun Institute of Optics, Fine Mechanics and Physics, Chinese Academy of Sciences, Changchun 130033, China*
[2]*University of Chinese Academy of Sciences, Beijing 100049, China*
Corresponding author: dingshaohang@126.com

A T-shaped altitude-azimuth mount is used as a platform for laser communication terminal equipment, and its pointing accuracy has an important influence on the link establishment, stable operation, and communication quality of laser communication. The bending deformation of the altitude axis is an important factor affecting the pointing accuracy of a T-shaped altitude-azimuth mount. In this paper, the bending deformation angle of the altitude axis caused by the load gravity was calculated by applying cantilever beam deformation theory, and the mathematical models of the pointing errors caused by bending deformation of the altitude axis were derived by using spherical trigonometry knowledge. Numerical simulations were conducted to analyze the laws of pointing errors. The simulation results show that the bending deformation angle has a great influence on the azimuth pointing error and the parallel error of the two collimation axes. Then two experimental platforms were established to validate the theoretical analyses. The experimental results are consistent with the theoretical results, which prove the correctness of the theoretical derivation. © 2019 Optical Society of America

https://doi.org/10.1364/AO.58.008141

1. INTRODUCTION

The laser has the advantages of strong confidentiality and anti-interference ability, high transmission rate and measurement accuracy, long working distance, small size, lightweight terminal equipment, low power consumption, etc. [1,2]. With the rapid development of modern technology, it is widely used in the work of high pointing precision optomechanical systems, e.g., gravity missions [3–5], optical links for unmanned aerial vehicle (UAV) applications [6], satellite laser communication [7–9], and underwater optical wireless communication [10,11]. As a promising laser application, laser communication plays a pivotal role in national defense and economic development and is also an important tool in future wars [12]. Pointing errors, which consist of two components, boresight and jitter, have a major impact on the laser communication link [13,14]. The pointing errors of a T-shaped altitude-azimuth mount, which is used as a platform for laser communication terminal equipment, will affect fast link establishment, high-speed transmission, and stable operation of laser communication. In [15–18], the different effects of boresight pointing errors on the performance of free-space optical communication were studied. Gawronski [19] presented the pointing error sources of large antennas and telescopes, including azimuth track imperfections and thermal

and wind forces. He also introduced several methods for pointing error correction, including lookup tables, conical scan, etc. In Ref. [20], the effects of localized deformation on pointing and tracking errors were researched, and the results could be used in the design of intersatellite optical communication systems. Tian *et al.* [21] researched the relationship between pointing error and temperature distribution of elliptical reflectors in intersatellite laser communication systems, and introduced the back-fixing method, which was proven to reduce pointing error. Han *et al.* [22] analyzed the orientation errors of an altitude-altitude (alt-alt) photoelectric telescope and the sensitivity of errors. An error correction model was built to improve the pointing precision. Feng *et al.* [23] gave an error elimination method to change the axis sloshing into parallel movement and proved its feasibility. Kaymak *et al.* [24] presented a survey on acquisition, tracking, and pointing (ATP) mechanisms used in free-space optical communication systems. They also discussed advantages and disadvantages of the surveyed ATP mechanisms. Vimal *et al.* [25] pointed out that satellite vibration resulted in serious pointing errors, thereby degrading communication performance, and suggested ways to tackle the effects of satellite vibration by optimizing the parameters of system design. Tian

_et al._ [26] described the three-axis error as the main factor affecting the accuracy of photoelectric theodolite angle measurement and deduced the mathematical models of the measurement errors caused by shafting errors.

The T-shaped altitude-azimuth mount has the advantages of small size, diversified load form, simple target acquisition, and servo control, etc. In this paper, the laser communication system with a T-shaped altitude-azimuth mount as the platform is used for communication between ground stations on the tops of mountains. The compound axis servo-mechanism, including a coarse-pointing main system and a fine-pointing subsystem is adopted, which has been applied [27,28]. The T-shaped altitude-azimuth mount rotates with terminals at a large angle to achieve coarse pointing, whereas the fast steering mirror (FSM) [29] installed in the terminal performs micromotion quickly to achieve fine pointing. The FSM has a small mass, and the T-shaped altitude-azimuth mount is in a static state or a low-speed motion state during the work. So, the effect of dynamic load on pointing can be neglected. This study focuses on the influence of load gravity. The impact of the bending deformation of altitude axis on the pointing of ordinary equipment is negligible, but not on photoelectric equipment with high pointing precision, especially when the altitude axis is relatively slender. The bending deformation of the altitude axis will bring the pointing error and prevent the terminals from pointing to the target smoothly. In this study, the mathematical models of pointing errors caused by the bending deformation of the altitude axis due to the load gravity are deduced, and the laws of pointing errors are analyzed and verified, which is helpful in correcting the pointing errors of laser communication. This study is of great theoretical significance and engineering value.

The rest of the paper is organized as follows: In Section 2, the dimensions and material of the altitude shaft studied are introduced. In Section 3, the formula for calculating the bending deformation angle of the altitude axis and the mathematical models of the pointing errors caused by the bending deformation of the altitude axis are deduced theoretically. The variation rules of pointing errors are described in Section 4. In Section 5, two experiments are proposed to prove the theoretical results. Finally, conclusions are drawn in Section 6.

2. DIMENSIONS AND MATERIAL OF THE ALTITUDE SHAFT

The research is carried out based on the altitude axis of the T-shaped altitude-azimuth mount in Fig. 1. The T-shaped altitude-azimuth mount has two rotating axes perpendicular to each other: the vertical azimuth axis and the horizontal altitude axis. A communication terminal that receives communication signals from a distant terminal and transmits communication signals to a distant terminal and a beacon terminal that transmits a beacon beam so that the distant terminal points to the correct location are mounted on the two ends of the altitude axis, respectively. The collimation axes of the two terminals are parallel and perpendicular to the altitude axis. The azimuth and altitude axes rotate cooperatively so that the two terminals point to the target. However, the bending deformation of the altitude axis will bring about the pointing error. The altitude shaft rotates with the left and right bearings as supports. Figure 2
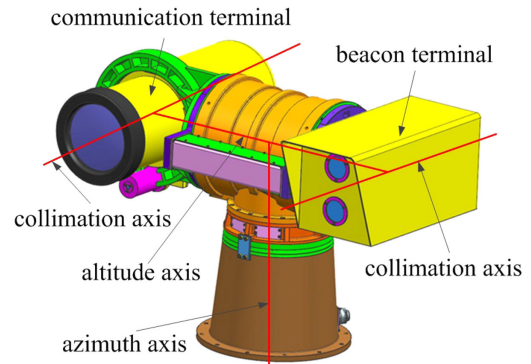
Fig. 1. T-shaped altitude-azimuth mount. The altitude axis and the collimation axes can rotate with the azimuth axis. The collimation axes can also rotate with the altitude axis. The target is determined by azimuth and altitude angles.
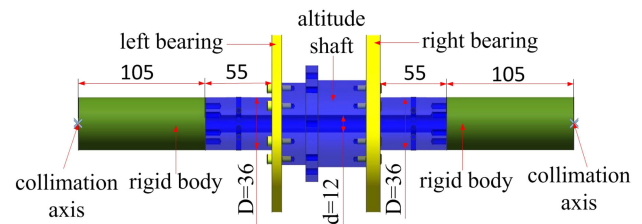

Fig. 2. Structure diagram of the altitude shaft. The center of gravity of the load at each end is located at the intersection of the altitude axis and the collimation axis. In this study, the threaded holes in the shaft and the deformation of the two terminals are ignored. The dimensions are given in units of millimeters.

shows the dimensions of the altitude shaft of the T-shaped altitude-azimuth mount, where the outer diameter of each end of the altitude shaft is $D = 36$ mm, the inner diameter is $d = 12$ mm, and the length of each cantilever is 55 mm. Both terminals are regarded as rigid bodies, and the collimation axes are both 105 mm away from the shaft end. The material of the shaft is steel 40Cr, which is suitable for the manufacture of shaft parts, and its modulus of elasticity is $E = 210$ GPa.

3. MATHEMATICAL MODELS OF POINTING ERRORS

Because of the minimal deformation of the high-precision bearing, it can be considered that the contact part between the altitude shaft and the inner ring surface of the bearing is fixed during the bending deformation of the altitude shaft. Consequently, both ends of the altitude axis can be simplified to cantilever beams. The two sides of the altitude shaft have the same shape and load weight, so take the left side as an example (Fig. 3). AB is a cantilever beam, BC is a rigid body, and C is the center of gravity of the load.

The existence of load gravity is equivalent to loading the concentrated force F in the vertical direction on Section C. The concentrated force F on Section C can be replaced by the concentrated force F and the bending moment $M = Fb$ acting on Section B.
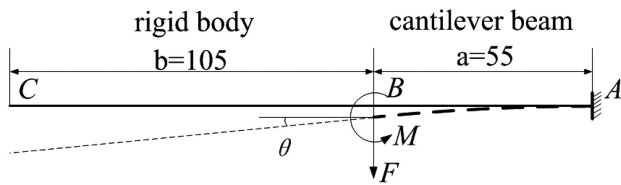
Fig. 3. Theoretical model of cantilever beam deformation. A is the position of the bearing, B is the end of the altitude axis, and C is the center of gravity of the load.

Because of the small deformation, the rotation angle θ of Section B is calculated by using the superposition method as follows:

$$\theta = \frac{Fa^2}{2EI} + \frac{Ma}{EI}, \tag{1}$$

where I is the second axial moment of area and can be calculated by

$$I = \frac{\pi(D^4 - d^4)}{6} 4. \tag{2}$$

By substituting $M = Fb$ into Eq. (1), we get

$$\theta = \frac{a^2 + 2ab}{2EI} F. \tag{3}$$

A. Altitude Pointing Error

Because the T-shaped altitude-azimuth mount is used for long-distance laser communication, the short distance between the collimation axis and the azimuth axis can be ignored, and it can be considered that the azimuth axis, the altitude axis, and the collimation axis intersect at one point. Figure 4 shows how the T-shaped altitude-azimuth mount with a bent altitude axis works. Line OZ is the azimuth axis, line $H_1 H_2$ is the ideal altitude axis, line OM is the ideal collimation axis, line $H_1' H_2'$ is the actual altitude axis, and line OM' is the actual collimation axis. $OZ' \perp$ plane $H_1' OM'$, and $\overset{\frown}{ZM}$ intersects $\overset{\frown}{Z'M'}$ at the target point A. The ideal collimation axis OM rotates around line $H_1 H_2$ by $\angle MOA$ to point A, whereas the actual collimation axis OM' rotates around line $H_1' H_2'$ by $\angle M'OA$ to point A. If $\angle ZOZ' = \Delta z$, $\angle MOM' = \Delta \alpha$, $\angle MOA = \beta$, and $\angle M'OA = \beta'$, we know that $\Delta z = \theta$, the azimuth pointing error is $\Delta \alpha$, and the altitude pointing error is $\Delta \beta = \beta' - \beta$.

In spherical $\triangle AMM'$, the following relationship can be obtained by using the sine formula of a spherical triangle,

$$\frac{\sin \angle AMM'}{\sin \overset{\frown}{AM'}} = \frac{\sin \angle AM'M}{\sin \overset{\frown}{AM}}. \tag{4}$$

Because $\angle AMM' = 90°$, $\overset{\frown}{AM'} = \beta'$, $\overset{\frown}{AM} = \beta$, and $\angle AM'M = 90° - \angle AM'Z = 90° - \Delta z$, we obtain the following relationship:

$$\sin \beta' = \frac{\sin \beta}{\cos \Delta z}. \tag{5}$$
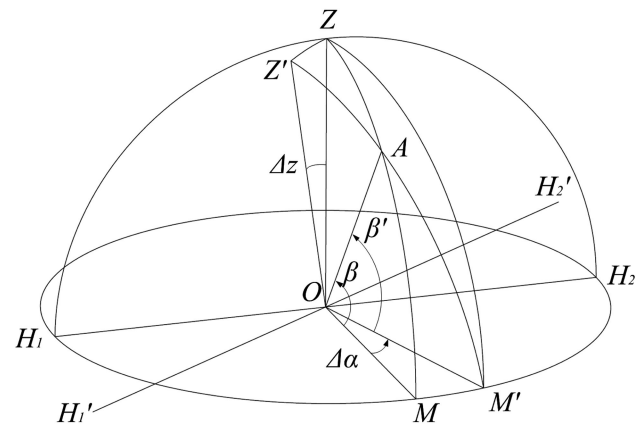
Fig. 4. Impact of the bending deformation of the altitude axis on pointing errors. Ideally, the collimation axis OM rotates around line $H_1 H_2$ along $\overset{\frown}{ZM}$. In fact, the collimation axis OM' rotates around line $H_1' H_2'$ along $\overset{\frown}{Z'M'}$.

Thus, the angle β' is calculated by using the following equation:

$$\beta' = \arcsin(\sin \beta \sec \Delta z). \tag{6}$$

By submitting $\Delta \beta = \beta' - \beta$ and $\Delta z = \theta$ into Eq. (6), we yield the following relationship:

$$\Delta \beta = \arcsin(\sin \beta \sec \theta) - \beta. \tag{7}$$

B. Azimuth Pointing Error

In spherical $\triangle AM'Z$, the following relationship can be obtained by using the sine formula of a spherical triangle:

$$\frac{\sin \angle AZM'}{\sin \overset{\frown}{AM'}} = \frac{\sin \angle AM'Z}{\sin \overset{\frown}{AZ}}. \tag{8}$$

As we know that $\angle AZM' = \Delta \alpha$, $\overset{\frown}{AM'} = \beta'$, $\angle AM'Z = \Delta z$, and $\overset{\frown}{AZ} = 90° - \beta$, we get the following relationship:

$$\frac{\sin \Delta \alpha}{\sin \beta'} = \frac{\sin \Delta z}{\cos \beta}. \tag{9}$$

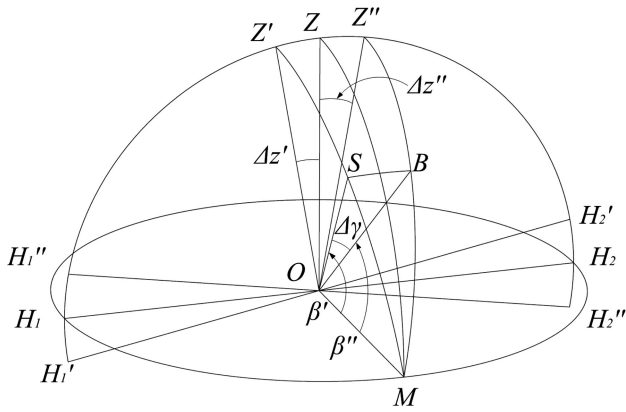By substituting Eq. (5) into Eq. (9), Eq. (9) can be transformed into

$$\sin \Delta \alpha = \tan \Delta z \tan \beta. \tag{10}$$

By substituting $\Delta z = \theta$ into Eq. (10), we can know

$$\Delta \alpha = \arcsin(\tan \theta \tan \beta). \tag{11}$$

C. Parallel Error of the Two Collimation Axes

The relationship between the two collimation axes is shown in Fig. 5. Line OZ is the azimuth axis, line $H_1 H_2$ is the ideal

Fig. 5. Impact of the bending deformation of the altitude axis on parallel error. Ideally, each of the collimation axes is the line OM that rotates around line $H_1 H_2$ along $\overset{\frown}{ZM}$. In fact, one collimation axis is the line OM that rotates around line $H_1' H_2'$ along $\overset{\frown}{Z'M}$, and the other collimation axis is the line OM that rotates around line $H_1'' H_2''$ along $\overset{\frown}{Z''M}$.

4. NUMERICAL SIMULATIONS

The mathematical models of the pointing errors caused by the bending deformation of the altitude axis are derived above. Next, numerical simulations of mathematical models are carried out to understand the influence degree of relevant parameters on pointing errors and the variation rules of pointing errors.

The T-shaped altitude-azimuth mount has a zenith blind zone, meaning that it does not work when β is around 90°. Numerical simulations were performed by taking the change of β within the range of 0°–85° and θ within the range of 0 deg $-20''$. Figure 6 shows that as the bending deformation angle θ and the target altitude angle β increase, the altitude pointing error $\Delta\beta$, the azimuth pointing error $\Delta\alpha$, and the parallel error $\Delta\gamma$ of the two collimation axes all increase. When $\theta = 10''$ and $\beta = 45°$, we can figure out that $\Delta\beta = 0.00024''$, $\Delta\alpha = 10.0''$, and $\Delta\gamma = 14.1''$; when $\theta = 20''$ and $\beta = 85°$, we can figure out that $\Delta\beta = 0.011''$, $\Delta\alpha = 228.6''$, and $\Delta\gamma = 39.8''$. The bending deformation angle θ has little effect on the altitude pointing error $\Delta\beta$, which is negligible in engineering applications, whereas the bending deformation angle θ has a great influence on the azimuth pointing error $\Delta\alpha$ and the

altitude axis, line OM is the collimation axis, line $H_1' H_2'$ is the actual altitude axis of the communication terminal, and line $H_1'' H_2''$ is the actual altitude axis of the beacon terminal. Line $H_1' H_2'$ and line $H_1'' H_2''$ are located in plane $H_1 Z H_2$, $OZ' \perp$ plane $H_1' H_2' M$, and $OZ'' \perp$ plane $H_1'' H_2'' M$. If line OM is the actual collimation axis of the communication terminal, it rotates around line $H_1'' H_2''$ by $\angle MOS$ to point S, and if line OM is the actual collimation axis of the beacon terminal, it rotates around line $H_1'' H_2''$ by $\angle MOB$ to point B. If $\angle ZOZ' = \Delta z'$, $\angle ZOZ'' = \Delta z''$, $\angle MOS = \beta'$, $\angle MOB = \beta''$, and $\angle BOS = \Delta\gamma$, then $\Delta z' = \Delta z'' = \theta$ and $\beta' = \beta''$ because of the symmetry of altitude axis structure and load weight. The parallel error of the two collimation axes is $\Delta\gamma$.

By using the cosine theorem of a spherical triangle in spherical $\triangle MBS$, we have

$$\cos \overset{\frown}{BS} = \cos \overset{\frown}{MS} \cos \overset{\frown}{MB} + \sin \overset{\frown}{MS} \sin \overset{\frown}{MB} \cos \angle BMS. \tag{12}$$

Because $\overset{\frown}{BS} = \Delta\gamma$, $\overset{\frown}{MS} = \beta'$, $\overset{\frown}{MB} = \beta''$, and $\angle BMS = \angle ZOZ' + \angle ZOZ'' = \Delta z' + \Delta z''$, we obtain the following relationship:

$$\cos \Delta\gamma = \cos \beta' \cos \beta'' + \sin \beta' \sin \beta'' \cos(\Delta z' + \Delta z''). \tag{13}$$

By substituting $\beta' = \beta''$ and $\Delta z' = \Delta z'' = \theta$ into Eq. (13), we can know

$$\cos \Delta\gamma = \cos^2\beta' + \sin^2\beta' \cos 2\theta. \tag{14}$$

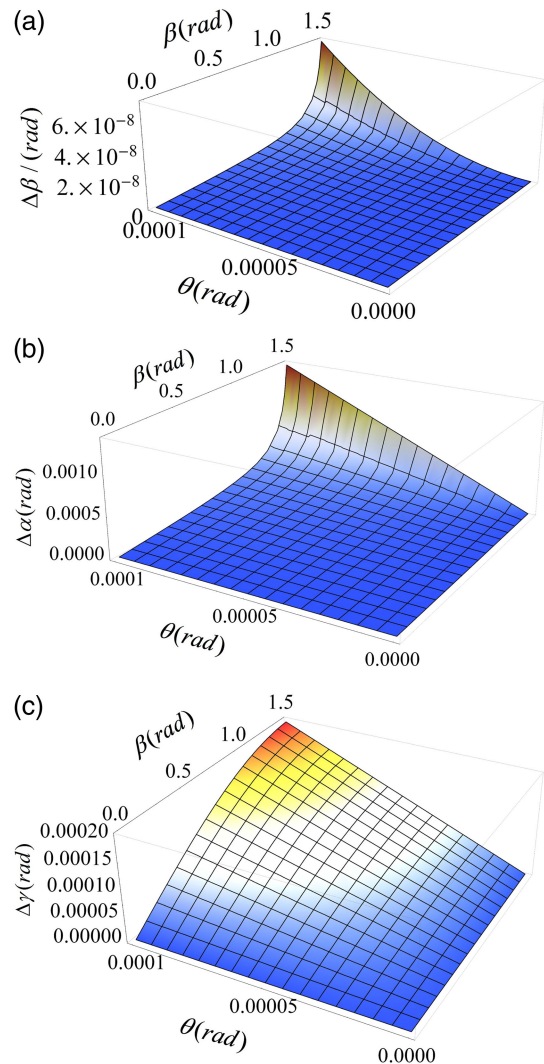By substituting Eq. (6) and $\Delta z = \theta$ into Eq. (14), we yield the following relationship:

$$\cos \Delta\gamma = 1 - 2\tan^2\theta \sin^2\beta, \tag{15}$$

$$\Delta\gamma = \arccos(1 - 2\tan^2\theta \sin^2\beta). \tag{16}$$

Fig. 6. Numerical simulation results. (a) $\Delta\beta - \theta - \beta$; (b) $\Delta\alpha - \theta - \beta$; (c) $\Delta\gamma - \theta - \beta$.

parallel error $\Delta\gamma$ of the two collimation axes. In particular, the influence on azimuth pointing error $\Delta\alpha$ increases sharply with the increase of the bending deformation angle θ and the target altitude angle β.

5. EXPERIMENTAL RESULTS AND DISCUSSION

It is very difficult to detect the pointing errors of a T-shaped altitude-azimuth mount by using the distant targets with known real azimuth and altitude angles. In this study, two experimental platforms that can be operated in the laboratory are built to verify the formula for calculating the bending deformation angle of the altitude axis and the mathematical models of the pointing errors caused by the bending deformation of the altitude axis, respectively. One experiment is to measure the bending deformation angle of the altitude axis by using an electronic theodolite and comparing it with the theoretical value. The other experiment is to measure the pointing errors by using a vertical row of point light sources as target points and comparing them with the theoretical pointing errors.

A. Bending Deformation Angle Experiment

The experimental platform (Fig. 7) is located in a constant temperature laboratory with a temperature of 26°C. Lock the azimuth axis so that it cannot rotate. A plane mirror is mounted at position A of one end of the altitude axis by using a connector. We turn off the lights in the lab, and then observe the plane mirror through an electronic theodolite (Leica TM6100A, 0.5″ accuracy). The laser emitted by the electronic theodolite returns to the electronic theodolite after being reflected by the plane mirror, and a reticle can be observed. We rotate the altitude axis to stabilize the reticle at the center by adjusting the plane mirror and the electronic theodolite. At this time, the normal line of the plane mirror is parallel to the center line of the altitude shaft, and the altitude angle reading of the electronic theodolite is t_1. Then, the terminals are installed on the two ends of the T-shaped altitude-azimuth mount. A hole is left on the terminal in order to prevent the plane mirror from being covered. Finally, the electronic theodolite is adjusted to center the reticle, and the altitude angle reading of the electronic theodolite is t_2 at this point. It can be analyzed that the bending deformation angle θ of the altitude axis is $\Delta t = t_2 - t_1$. If Δt is stable during the rotation of the altitude axis and is consistent with the result of Eq. (3), we consider that the relevant theoretical derivation above is correct.
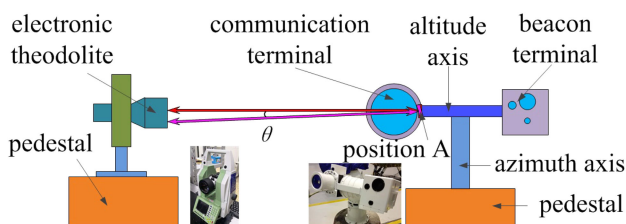
Fig. 7. Principle of bending deformation angle experiment. The electronic theodolite, which is an angle measuring instrument, can measure the bending deformation angle of the altitude axis caused by the load.
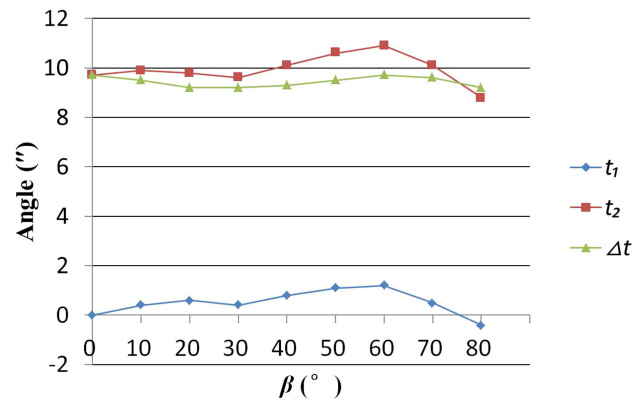

Fig. 8. Results of the bending deformation angle experiment. Angle t_1 and angle t_2 are the readings of the electronic theodolite before and after loading, respectively. $\Delta t = t_2 - t_1$.

The actual weight of the communication terminal and the actual weight of the beacon terminal determine that the single side load weight of the altitude axis is 10 kg, which means $F = 98$N. The experimental results of t_1, t_2, and Δt are shown in Fig. 8 based on the above measurement principle. Since the altitude axis itself wobbles, t_1 changes slightly with the increase of target altitude, angle β. The altitude axis is bent after the loads are installed, and t_2 changes around 10″. The average of a series of Δt is 9.43″. We substitute $F = 98$N into Eq. (3) and get $\theta = 4.17 \times 10^{-5}$ rad $= 8.61″$. There is a difference between the experimental results and the theoretical result because of the existence of threaded holes, position error of the center of gravity, electronic theodolite error, installation error, personnel error, etc. Comparing the average of Δt with θ, the error between them is 9.5%, which is relatively small. This experiment proves that the theoretical results are of high accuracy.
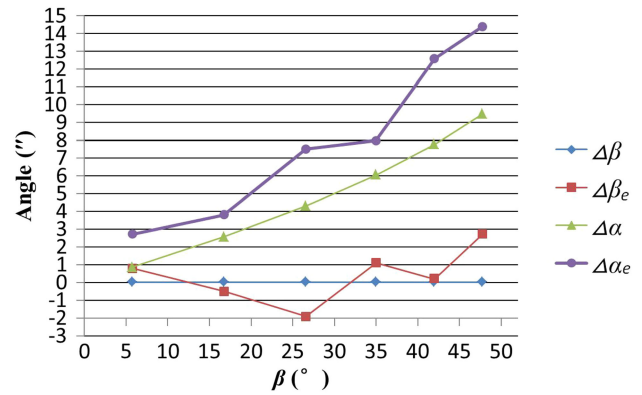
B. Pointing Error Experiment

The position relationship between the point light source and the T-shaped altitude-azimuth mount is shown in Fig. 9. The metal support is made of aluminum alloy tube and has good stability. There are a series of pinholes in the metal support to suspend the point light source. The height of the point light source on the metal support can be adjusted by using different pinholes. The position tolerance of the pinholes is ±0.02 mm. Place the metal support at a distance from the T-shaped altitude-azimuth mount. First, the point light source is suspended at the bottom and top of the metal support, respectively, by using the pinhole positioning method. The coordinate of point light source is measured simultaneously with two electronic theodolites. By repeatedly measuring the angle and adjusting the metal support, the azimuth coordinates of the point light source located in two positions remain almost constant. The metal support is considered vertical at this time. Next, the communication terminal aims at the point light source located at point 1 after leveling the T-shaped altitude-azimuth mount. By adjusting the height of the T-shaped altitude-azimuth mount, the altitude angle of the communication terminal is zero. The azimuth and altitude angle readings at this time are recorded by the encoders installed
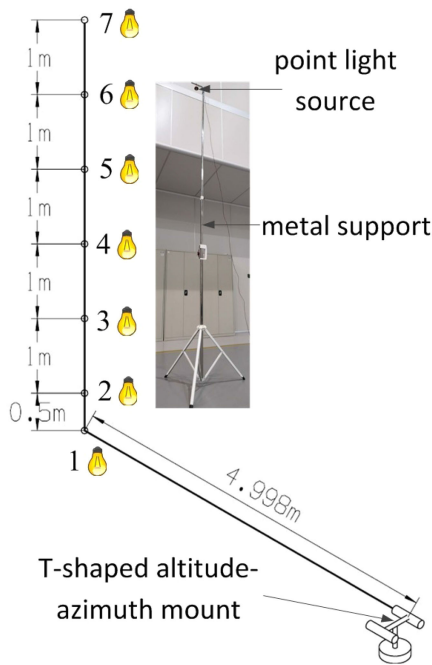
Fig. 9. Principle of the pointing error experiment. The collimation axis of the communication terminal is horizontal when the target is point 1. Points 1–7 are located on a vertical line. The point light source is sequentially placed at points 1–7. The experimental values of azimuth and altitude angles of the T-shaped altitude-azimuth mount can be obtained when the communication terminal aims at the point light source.

in the T-shaped altitude-azimuth mount. According to the theoretical analysis results, it can be considered that both angle values at this time are real angle values, and there is almost no error. The distance from point 1 to the altitude axis is 4.998 m and the distance error is ±0.5 mm. Then, the metal support remains stationary, and the point light source is sequentially placed at points 2–7. The azimuth angle α_e and altitude angle β_e readings of the T-shaped altitude-azimuth mount are recorded. According to the positional relationship in Fig. 9, the real azimuth angle α and altitude angle β of points 2–7 can be calculated. The azimuth angle experimental error $\Delta\alpha_e = \alpha_e - \alpha$ and the altitude angle experimental error $\Delta\beta_e = \beta_e - \beta$ can be obtained by comparing α_e and α, β_e, and β. Finally, the azimuth angle theoretical error $\Delta\alpha$ and the altitude angle theoretical error $\Delta\beta$ of points 2–7 can be calculated by Eqs. (7) and (11).

Figure 10 shows the experimental results based on the above experimental principle. $\Delta\beta$ is very small, almost zero, while $\Delta\beta_e$ changes around zero. $\Delta\alpha_e$ and $\Delta\alpha$ have the same trend. There exist errors between the experimental results and the theoretical results due to threaded holes in the altitude shaft, altitude axis wobbling, vertical error of the metal support, position tolerance of pinholes in the metal support, perpendicularity error between the collimation axis and the altitude axis, encoder reading error, etc. The maximum error between $\Delta\beta_e$ and $\Delta\beta$ is 2.7″. The maximum error between $\Delta\alpha_e$ and $\Delta\alpha$ is 4.9″. These errors are relatively small, which proves that the theoretical results are correct.

Fig. 10. Results of the pointing error experiment. $\Delta\beta$ is the theoretical error of the altitude angle calculated by Eq. (7), $\Delta\beta_e$ is the experimental error of the altitude angle, $\Delta\alpha$ is the theoretical error of the azimuth angle calculated by Eq. (11), and $\Delta\alpha_e$ is the experimental error of the azimuth angle.

6. CONCLUSION

In this paper, based on the high-precision T-shaped altitude-azimuth mount of laser communication, the formula for calculating the bending deformation angle of the altitude axis and the mathematical models of the pointing errors caused by the bending deformation of altitude axis were deduced theoretically, and the effects of the bending deformation of the altitude axis on the pointing errors were analyzed. The numerical simulation results show that the altitude pointing error, the azimuth pointing error, and the parallel error of the two collimation axes all increase as the bending deformation angle and the target altitude angle increase. In addition, the bending deformation angle has little influence on the altitude pointing error, but has a great influence on the azimuth pointing error and the parallel error of the two collimation axes. The bending deformation angle of the altitude axis was basically stable with the change of the altitude angle during the bending deformation angle experiment, and the error between it and the theoretical result is 9.5%. In the pointing error experiment, the maximum difference between experimental error and theoretical error of altitude angle is 2.7″, and the maximum difference between experimental error and theoretical error of azimuth angle is 4.9″. These experimental results verify the correctness of the theoretical results. This study provides a theoretical basis for the correction of the pointing errors caused by the bending deformation of the altitude axis of a T-shaped altitude-azimuth mount.

REFERENCES

1. H. Kaushal and G. Kaddoum, "Optical communication in space: challenges and mitigation techniques," IEEE Commun. Surv. Tuts. **19**, 57–96 (2016).
2. M. A. Khalighi and M. Uysal, "Survey on free space optical communication: a communication theory perspective," IEEE Commun. Surv. Tuts. **16**, 2231–2258 (2014).

3. H. C. Yeh, Q. Z. Yan, Y. R. Liang, Y. Wang, and J. Luo, "Intersatellite laser ranging with homodyne optical phase locking for space advanced gravity measurements mission," Rev. Sci. Instrum. **82**, 044501 (2011).

4. Y. Luo, H. Li, and H. C. Yeh, "Note: digital laser frequency auto-locking for inter-satellite laser ranging," Rev. Sci. Instrum. **87**, 056105 (2016).

5. J. Y. Zhang, M. Ming, Y. Z. Jiang, H. Z. Duan, and H. C. Yeh, "Inter-satellite laser link acquisition with dual-way scanning for space advanced gravity measurements mission," Rev. Sci. Instrum. **89**, 064501 (2018).

6. C. Chen, A. Grier, M. Malfa, E. Booen, H. Harding, C. Xia, M. Hunwardsen, J. Demers, K. Kudinov, and G. Mak, "High-speed optical links for UAV applications," in *Free-Space Laser Communication and Atmospheric Propagation XXIX* (International Society for Optics and Photonics, 2017), p. 1009615.

7. A. Biswas, J. M. Kovalik, M. Srinivasan, M. Shaw, S. Piazzolla, M. W. Wright, and W. H. Farr, *Deep Space Laser Communications* (SPIE LASE, 2016).

8. Z. J. Liu, J. Y. Zhang, J. Dou, Q. Guo, Y. Gao, and L. Jin, "Enlightenment for the development of foreign satellite laser communication technology," in *Fiber Optic Sensing and Optical Communication* (2018), p. 108490J.

9. Q. Wang, Y. F. Liu, J. Ma, L. Y. Tan, S. Y. Yu, and C. J. Li, "Quick acquisition and recognition method for the beacon in deep space optical communications," Appl. Opt. **55**, 9738–9743 (2016).

10. Z. Vali, A. Gholami, Z. Ghassemlooy, M. Omoomi, and D. G. Michelson, "Experimental study of the turbulence effect on underwater optical wireless communications," Appl. Opt. **57**, 8314–8319 (2018).

11. L. J. Johnson, R. J. Green, and M. S. Leeson, "Underwater optical wireless communications depth-dependent beam refraction," Appl. Opt. **53**, 7273–7277 (2014).

12. M. R. Ci, J. J. Liu, L. Han, and J. Y. Chen, "Optical fiber laser phased array technology for space laser communication," in *Optical Sensing and Imaging Technologies and Applications* (2018), p. 108462Y.

13. D. K. Borah and D. G. Voelz, "Pointing error effects on free-space optical communication links in the presence of atmospheric turbulence," J. Lightwave Technol. **27**, 3965–3973 (2009).

14. X. Yi and M. W. Yao, "Free-space communications over exponentiated Weibull turbulence channels with nonzero boresight pointing errors," Opt. Express **23**, 2904–2917 (2015).

15. P. Wang, X. X. Liu, T. Cao, H. H. Fu, R. R. Wang, and L. X. Guo, "Impact of nonzero boresight pointing errors on the performance of a relay-assisted free-space optical communication system over exponentiated Weibull fading channels," Appl. Opt. **55**, 7593–7603 (2016).

16. Z. G. Gao, H. Z. Liu, X. P. Ma, and W. Lu, "Performance of multi-hop parallel free-space optical communication over gamma-gamma fading channel with pointing errors," Appl. Opt. **55**, 9178–9184 (2016).

17. R. Boluda-Ruiz, A. García-Zambrana, B. Castillo-Vázquez, and C. Castillo-Vázquez, "Impact of nonzero boresight pointing error on ergodic capacity of MIMO FSO communication systems," Opt. Express **24**, 3513–3534 (2016).

18. A. García-Zambrana, C. Castillo-Vázquez, B. Castillo-Vázquez, and R. Boluda-Ruiz, "Bit detect and forward relaying for FSO links using equal gain combining over gamma-gamma atmospheric turbulence channels with pointing errors," Opt. Express **20**, 16394–16409 (2012).

19. W. Gawronski, "Control and pointing challenges of large antennas and telescopes," IEEE Trans. Control Syst. Technol. **15**, 276–289 (2007).

20. Y. Q. Yang, L. Y. Tan, and J. Ma, "Pointing and tracking errors due to localized distortion induced by a transmission-type antenna in intersatellite laser communications," Appl. Opt. **48**, 786–791 (2009).

21. L. Y. Tan, Y. W. Song, J. Ma, S. Y. Yu, Q. Q. Han, Y. J. Jiang, J. Wang, and S. Fu, "Pointing error due to temperature distribution of SiC reflectors in intersatellite laser communications," Appl. Opt. **49**, 4168–4174 (2010).

22. X. B. Han, J. X. Zhang, J. Y. Zhao, Z. Wang, Y. D. Song, Z. C. Wang, Y. Z. Zhao, and X. X. Wu, "Forecast for orientation errors of alt-alt photo-electric telescope," Opt. Precis. Eng. **18**, 1595–1604 (2010).

23. D. Y. Feng, Y. G. Gao, and W. B. Zhang, "Elimination of shafting errors in photoelectric theodolites with standard-bearings," Opt. Precis. Eng. **19**, 605–611 (2010).

24. Y. Kaymak, R. Rojas Cessa, J. H. Feng, N. Ansari, M. C. Zhou, and T. R. Zhang, "A survey on acquisition, tracking, and pointing mechanisms for mobile free-space optical communications," IEEE Commun. Surv. Tuts. **20**, 1104–1123 (2018).

25. K. Vimal and S. Prince, "System analysis for optimizing various parameters to mitigate the effects of satellite vibration on inter-satellite optical wireless communication," in *IEEE International Conference on Signal Processing, Informatics, Communication and Energy Systems* (2015), pp. 1–4.

26. L. D. Tian, C. H. Liu, J. K. Zhao, P. Liang, Y. X. Duan, and Z. F. Zhang, "Impact of three-axis error on angle measurement of photoelectric theodolite," Infrared Laser Eng. **42**, 192–197 (2013).

27. A. Carrasco-Casado, R. Vergaz, J. M. Sanchez-Pena, E. Oton, M. A. Geday, and J. M. Oton, "Low-impact air-to-ground free-space optical communication system design and first results," in *International Conference on Space Optical Systems and Applications* (2011), pp. 109–112.

28. J. R. Rzasa, "Pointing, acquisition, and tracking for directional wireless communications networks," Ph.D dissertation (University of Maryland, 2012).

29. Y. Ni, J. Wu, X. San, S. Gao, S. Ding, J. Wang, and T. Wang, "Deflection angle detecting system for the large-angle and high-linearity fast steering mirror using quadrant detector," Opt. Eng. **57**, 024110 (2018).